


**Quantum lock-in detection of a vector light shift**Kosuke Shibata<sup>✉,\*</sup>, Naota Sekiguchi, and Takuya Hirano*Department of Physics, Gakushuin University, Tokyo 171-8588, Japan* (Received 25 January 2021; accepted 15 April 2021; published 30 April 2021)

We demonstrate detection of a vector light shift (VLS) using the quantum lock-in method. The method offers precise VLS measurement with little affect from real magnetic field fluctuation. We detect a VLS on a Bose-Einstein condensate (BEC) of  $^{87}\text{Rb}$  atoms caused by an optical trap beam with a resolution less than 1 Hz. We demonstrate the elimination of a VLS by controlling the beam polarization to realize a long coherence time of an  $F = 2$  BEC in the stretched state. Quantum lock-in VLS detection should find wide application, including the study of spinor BECs, electric dipole moment searches, and precise magnetometry.

DOI: [10.1103/PhysRevA.103.043335](https://doi.org/10.1103/PhysRevA.103.043335)**I. INTRODUCTION**

The ac Stark shift or light shift plays a significant role in atomic physics. One example is the optical trap [1], which has been extensively used in cold-atom experiments and has been the subject of intriguing and important research, including low-dimensional [2] and uniform gases [3] and atoms in an optical lattice with applications in quantum simulation [4] and atomic clocks [5,6]. It has also enabled the study of multicomponent gases and in particular spinor Bose-Einstein condensates (BECs) [7].

The light shift has vector and tensor components and hence is state dependent in general [8–10]. The state dependence has been exploited for realizing state-selective transport [11,12] and confinement [13]. However, a state-dependent shift is often undesirable for situations in which well-controlled spin evolution is required. Escaping from a vector light shift (VLS), which is equivalent to a *fictitious* magnetic field, has been an important issue in precise measurements, such as the search for an atomic electric dipole moment [14] and exotic spin-dependent interactions [15]. Reducing the VLS is also important in atomic magnetometers, in which the VLS introduces systematic errors. The quantum noise associated with the light shift due to the probe field ultimately limits the sensitivity [16].

The VLS restricts the potential use of optically trapped atoms for magnetically sensitive experiments. While its effect can be diminished by applying a bias magnetic field in a direction orthogonal to the wave vector, the VLS can still be a significant noise source in precise measurements [14]. It is necessary to reduce the VLS when an ultralow magnetic field is required. In addition, the relative direction cannot be chosen satisfactorily in some situations, such as in three-dimensional optical lattice experiments.

In order to eliminate the VLS caused by optical trapping beams, the light polarization should be precisely controlled, because the VLS is proportional to the intensity of a circularly

polarized component [1,8–10]. However, it is a formidable task to precisely extinguish the circular component at the atom position located in a vacuum cell. Polarization measurements and control outside the cell do not ensure the degree of linear polarization due to the stress-induced birefringence of the vacuum windows [17].

Therefore, a sensitive and robust polarization measurement method using atoms themselves as a probe is important. Most effective polarization measurements are accomplished by using atoms themselves as a probe. Polarization measurements with an atomic gas have been performed with various methods including Larmor precession measurement [18], precise microwave spectroscopy [19], and frequency modulation nonlinear magneto-optical rotation [20]. Differential Ramsey interferometry has been developed for spinor condensates [21]. Polarization measurements by fluorescence detection have been recently demonstrated for ions [22].

In this paper we demonstrate VLS detection by applying the quantum lock-in method [23,24], which is immune to environmental magnetic field noise and thus achieves excellent accuracy in VLS detection. The quantum lock-in detection has several advantages over other methods [23,24]. It belongs to the ac detection method and offers better results than the dc ones, which tends to suffer from large noises at dc or low frequencies. Compared with other ac methods, the narrow detection bandwidth offers a better signal-to-noise (S/N) ratio, as in the classical lock-in detection. Furthermore, the frequent spin inversion (bang-bang control) in the lock-in detection is helpful in reducing the undesired spin evolution in a cold-atom gas under a (real or fictitious) magnetic field gradient [25]. We detect a VLS induced by an optical trap beam on a BEC of  $^{87}\text{Rb}$  atoms with a resolution less than 1 Hz. This detection method is feasible to implement and should have wide applications in various research areas involved with optical fields.

The paper is organized as follows. In Sec. II our experimental method and setup are presented. The experimental results are described in Sec. III. We discuss the applications and potential performance of the quantum lock-in VLS detection in Sec. IV. We summarize the paper in Sec. V.

\*shibata@qo.phys.gakushuin.ac.jp

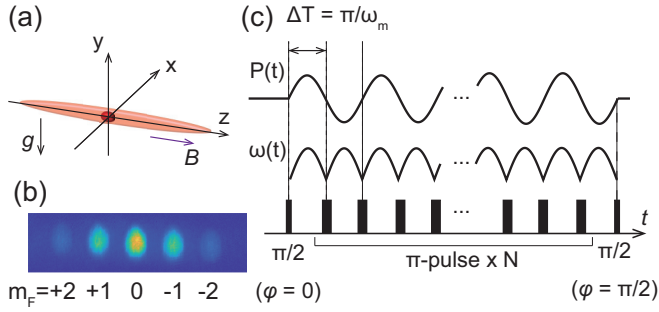


FIG. 1. (a) Experimental configuration. A BEC is trapped in the axial trap beam along the  $z$  axis and the radial trap beam along the  $x$  axis (not shown). (b) Typical TOF image of a BEC measured after rf pulses for the detection. The spin components ( $m_F = -2, -1, 0, 1, 2$ ) are spatially resolved by the Stern-Gerlach method. (c) Time sequence for the quantum lock-in detection of a VLS. The beam power  $P(t)$  is modulated with a frequency  $\omega_m$ . The phase of the spin vector evolves with an angular frequency of  $\omega(t)$ . The accumulated phase  $\Phi = \int_0^T \omega(t) dt$  is finally measured.

## II. EXPERIMENTAL METHOD AND SETUP

We produce a BEC in a vacuum glass cell. A BEC of  $3 \times 10^5$  atoms in the hyperfine spin  $F = 2$  state is trapped in a crossed optical trap. The trap consists of an axial beam at a wavelength of 850 nm and a radial beam at 1064 nm. The axial and radial beam waists are approximately equal to 30 and 70  $\mu\text{m}$ , respectively. The typical axial and radial trapping frequencies are  $2\pi \times 160$  and  $2\pi \times 12$  Hz, respectively, and the Thomas-Fermi radii are 4.0 and 52  $\mu\text{m}$ . A magnetic bias field  $B$  of 15  $\mu\text{T}$  is applied along the axial beam to define the quantization axis, as shown in Fig. 1(a). The atoms are initially in the  $|F, m_F\rangle = |2, 2\rangle$  state, where  $m_F$  denotes the magnetic sublevel. The ellipticity of the axial beam at the atomic position is controlled with a quarter waveplate (QWP) in the VLS measurement described below. The QWP is located between a polarization beam splitter for polarization cleaning and the cell. The angle of the QWP is adjusted with a precise manual rotation stage. The minimum scale of the rotation stage is 0.28 mrad.

The time sequence for the quantum lock-in detection of a VLS is shown in Fig. 1(c). The lock-in technique enables enhanced sensitivity at the modulation frequency while reducing the effect of unwanted noise. We measure a VLS induced by the axial optical trap beam with multiple rf pulses. The trap beam power  $P(t)$  is modulated with a frequency  $\omega_m$  during the pulse application as

$$P(t) = P_0[1 + p \sin(\omega_m t)] \equiv P_0 + P_1 \sin(\omega_m t), \quad (1)$$

where  $P_0$  is the mean power and  $p$  is the modulation index. Here  $P_1$  can be negative by changing the modulation phase by  $\pi$ .

The frequency  $\omega_m$  should be set to avoid parametric heating of the atoms. We use  $\omega_m$  sufficiently higher than twice the trapping frequency. In addition, the background magnetic field noise at  $\omega_m$  needs to be small. Therefore, optimal  $\omega_m$  should strongly depend on the environmental noise. The multiple of the ac line frequency (50 Hz in our experiment) at low frequencies is not used in our experiment. While higher

modulation frequency is expected to be better to avoid low-frequency noises, an upper limit is posed due to a finite rf pulse width. Due to the available rf power, we cannot make the  $\pi/2$  pulse shorter than approximately 10  $\mu\text{s}$ . In each experiment, we try several modulation frequencies to obtain a good S/N ratio, taking the above requirements into account. The modulation generates an ac fictitious magnetic field to be measured, given by

$$B_{\text{fic}} = -\frac{1}{4}\alpha^{(1)}\mathcal{C}I_1 \sin(\omega_m t) \equiv B_1 \sin(\omega_m t), \quad (2)$$

where  $\alpha^{(1)}$  is the ac vector polarizability,  $\mathcal{C}$  is the degree of the circularity, and  $I_1$  is the beam intensity corresponding to  $P_1$ .

The rf pulse set consists of an initial  $\pi/2$  pulse at  $t = 0$ , an odd number  $N$  of  $\pi$  pulses, and a readout  $\pi/2$  pulse. The pulses are equally spaced by  $\Delta T$ . The spacing satisfies  $\omega_m = \pi/\Delta T$  so that the evolved phase due to the fictitious field is constructively accumulated. The relative phase  $\Delta\varphi$  between the initial and readout pulses is set to  $\pi/2$  for maximum sensitivity to small changes in the accumulated phase  $\Phi$ , which is explicitly given by

$$\Phi = \frac{2}{\pi} \frac{g_F \mu_B B_1}{\hbar} T \equiv \frac{2}{\pi} \omega_1 T, \quad (3)$$

where  $g_F$  is the Landé  $g$  factor,  $\mu_B$  is the Bohr magneton,  $\hbar$  is the reduced Planck constant, and  $T = (N + 1)\Delta T$  is the phase accumulation time. In addition,  $\omega_1/2\pi$  represents the VLS corresponding to  $B_1$  in units of frequency.

The readout pulse converts  $\Phi$  into the magnetization  $m$  as

$$m \equiv \frac{\sum_i i N_i}{N_{\text{tot}}} = \mathcal{V} F \sin \Phi, \quad (4)$$

where  $N_i$  is the atom number in the  $|F, m_F = i\rangle$  state ( $i = -2, -1, 0, 1, 2$ ) after the readout pulse,  $N_{\text{tot}} = \sum_i N_i$  is the total atom number, and  $\mathcal{V}$  is the visibility. Here  $\mathcal{V}$  is ideally 1, but in practice it is less than 1 due to magnetic field noise [23]. Imperfections in the initial state preparation and spin manipulation also decrease  $\mathcal{V}$ . The magnetization is measured by standard absorption imaging after a time of flight with Stern-Gerlach spin separation [see Fig. 1(b)].

## III. RESULTS

We first confirm the validity of the detection scheme. We perform a lock-in detection with  $\omega_m = 2\pi \times 2$  kHz ( $\Delta T = 0.25$  ms) and  $N = 27$ , and hence  $T = 7$  ms. The mean power  $P_0$  is fixed to 11 mW. The change in  $m$  is observed as  $p$  is varied. The result is plotted in Fig. 2. Here the angle of the QWP axis,  $\theta$ , is approximately  $4^\circ$  apart from the optimal angle  $\theta^*$  minimizing the VLS. The experimental determination of  $\theta^*$  is described below. Here  $m$  is well fitted by a sinusoidal function  $\mathcal{V} F \sin ap$ , indicating the VLS was successfully detected. The visibility in this detection setting is found to be  $\mathcal{V} = 0.746(42)$  from an independent measurement with no modulation ( $p = 0$ ) where  $\Delta\varphi$  is scanned.

The detection is used to minimize the VLS. We control the VLS by changing  $\theta$  with  $p$  fixed to 0.32. The  $\theta$  dependence of  $m$  is shown in Fig. 3(a). Because  $\mathcal{C} \approx \sin 2(\theta - \theta^*) \equiv \sin 2\Delta\theta$  when the birefringence in the optical path is small [21] and  $|\Delta\theta| \ll 1$ , we fit  $m$  by  $\mathcal{V} F \sin \beta_1(\theta - \theta^*)$ . The fit gives  $\beta_1 = 6.2(2)$ , which is in reasonable agreement with

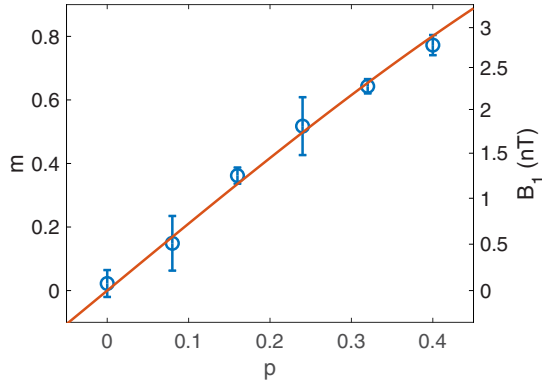


FIG. 2. Detected magnetization after the rf pulses. The error bars represent the sample standard deviation. The red solid line is the fitting curve by  $V\mathcal{F} \sin ap$ . The right axis represents  $B_1$ , corresponding to the magnetization. It should be noted that the right axis scale is not linear since  $B_1$  is proportional to  $\arcsin \frac{m}{V\mathcal{F}}$ .

the calculation. Here  $\theta^*$  is found to be  $-(6.6 \pm 1.1)$  mrad. The VLS resolution is evaluated as  $\delta\omega = \beta_1 \delta\theta^*/T = 2\pi \times 0.16$  Hz, where  $\delta\theta^*$  is the uncertainty in the  $\theta^*$  estimation.

We perform a fine estimation of  $\theta^*$  by extending  $T$  to 27.2 ms and applying a larger modulation. In this experiment,  $\omega_m = 2\pi \times 625$  Hz and  $N = 33$ . While large  $T$  (or  $N$  if  $\omega_m$  is fixed) should in principle offer a better S/N ratio, we observe significant fluctuation of the background signal ( $m$  without

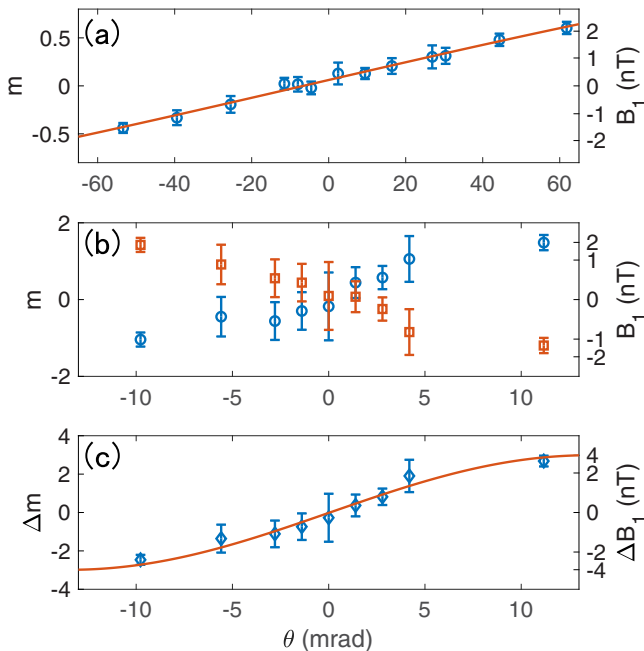


FIG. 3. Polarization dependence of the magnetization signal. (a) Measurement result with  $T = 7$  ms. (b) Measurement result with  $T = 28.2$  ms. The blue circles and red squares represent  $m_+$  and  $m_-$ , respectively. (c) Plot of  $\Delta m$  as a function of  $\theta$ . Here  $\Delta B_1$  is the difference between the fictitious magnetic fields for positive and negative  $P_1$ . The solid lines in (a) and (c) are the fitting curves of  $a \sin b(\theta - \theta^*)$  (see the text for details). The error bars represent the standard deviation.

optical intensity modulation) for larger  $N$ , possibly due to imperfectness of the spin control by rf pulses. Low  $\omega_m$  is chosen to make  $T$  longer for better sensitivity, under the restrictions that the parametric heating is not induced and the background magnetic field fluctuation at  $\omega_m$  is quiet, as mentioned above.

We measure  $m$  for  $P_1 = \pm 13$  mW, referred to as  $m_{\pm}$ , respectively. In finding  $\theta^*$ , we use  $\Delta m = m_+ - m_-$  to cancel the offset due to the background field and the systematic error in the spin measurement. The results are shown in Figs. 3(b) and 3(c). Here  $\Delta m$  is fitted by  $4V\mathcal{F} \sin \beta_2(\theta - \theta^*)$ , giving  $\beta_2 = 117(16)$  and  $\theta^* = (0.1 \pm 0.4)$  mrad. The angle resolution is improved 2.8 times.

We observe a larger variance in  $m$  in the experiments for the fine  $\theta^*$  estimation. The standard deviation of  $\Delta m$  is on average 0.64, while that for the reference data without modulation is 0.09. Therefore, a further improvement by a factor of at least 7 is possible, because  $\Delta m$  should ideally be independent of  $T$  and the modulation strength. We ascribe the increased variance to the actual variation of the vector shift over the experimental runs, caused by beam polarization fluctuation. The result of the sensitive detection implies that the beam circularity varies with a standard deviation of approximately  $3 \times 10^{-3}$ . On the other hand, from an independent experiment, we expect that the retardance of the QWP should vary by several milliradians due to the temperature change in our experimental room (within approximately 0.6 K with a period of around 20 min).

The BEC is subject to a fictitious magnetic field gradient without the VLS cancellation, because it is located at the shoulder of the optical trap beam due to gravity sag. While the observed fictitious magnetic field is small, the gradient in the fictitious field can be on the order of  $100 \mu\text{T}/\text{m}$ . The gradient displaces the trap potential for each spin state other than the  $m_F = 0$  state, thereby driving spin-dependent motion. We observe an actual motion in a transversally stretched BEC in the hyperfine spin  $F = 2$  state, prepared after the initial  $\pi/2$  pulse. We plot the vertical displacement of the spin components in the TOF image, which reflects the momentum, in Figs. 4(a)–4(d). The direction of the motion inverts depending on the sign of  $\Delta\theta$  and the motion becomes small at  $\Delta\theta \approx 0$ . These observations indicate that the motion is induced by the fictitious magnetic field.

The fictitious magnetic field gradient also causes nonlinear spin evolution and thus a population change, as does the real magnetic field gradient [25]. The initial stretched atomic spin state breaks due to the spin mixing seeded by the nonlinear spin evolution. We observe vertical separation of spin components during this process. This observation is consistent with the fact that the vertical size of our BEC is slightly larger than the spin healing length  $\xi_s$ . We estimate  $\xi_s = \sqrt{7/8\pi(a_4 - a_2)n} = 3.7 \mu\text{m}$ , where  $a_{\mathcal{F}}$  is the  $s$ -wave scattering length for the collisional channel of the total angular momentum  $\mathcal{F}$  and  $n$  is the mean atomic density. Even so, the break of the stretched state can be inferred from the global population change. We show  $p_0 = N_0/N_{\text{tot}}$ ,  $p_1 = (N_{-1} + N_{+1})/2N_{\text{tot}}$ , and  $p_2 = (N_{-2} + N_{+2})/2N_{\text{tot}}$  in Figs. 4(e)–4(h). The population changes are observed at an earlier time ( $t < 100$  ms) except for the case  $\Delta\theta \approx 0$ . These changes can be attributed to the fictitious magnetic field gradient. The faster population change for  $\Delta\theta = 4^\circ$  is consistent with a

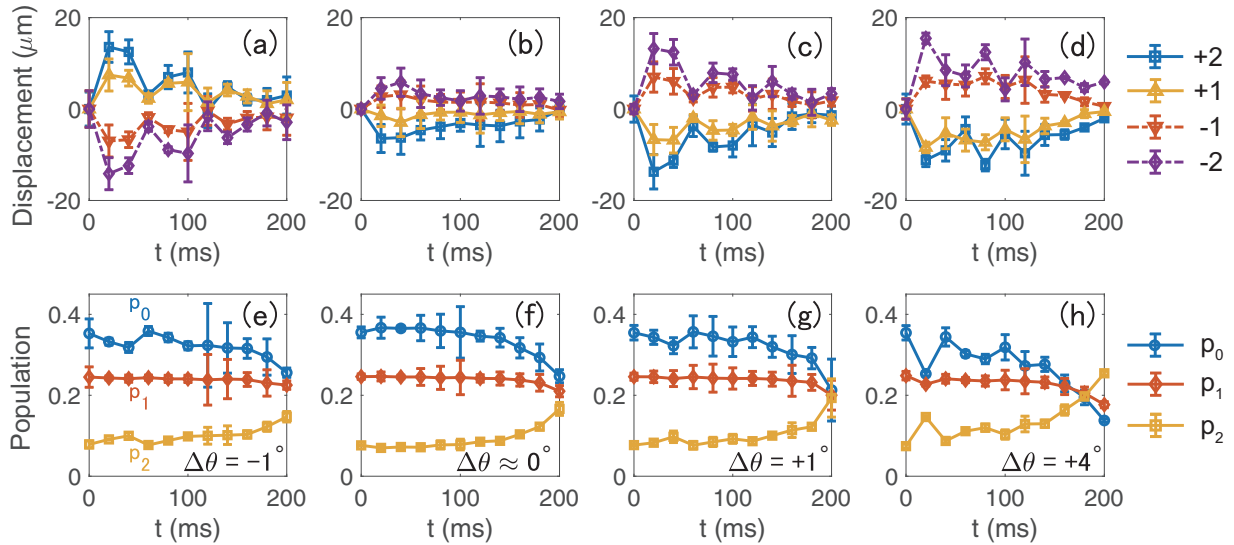


FIG. 4. Effects of the fictitious magnetic field on a transversally polarized BEC. The vertical displacement of the center of mass in the TOF image is plotted for (a)  $\Delta\theta = -1^\circ$ , (b)  $\Delta\theta = 0.02^\circ$ , (c)  $\Delta\theta = 1^\circ$ , and (d)  $\Delta\theta = 4^\circ$ . The solid and dashed lines are guides for the eyes. (e)–(h) Population evolution corresponding to (a)–(d). The values of  $p_0$  (blue circles),  $p_1$  (red diamonds), and  $p_2$  (yellow squares) are shown ( $p_i$  is defined in the text). The error bars represent the standard deviations.

qualitative estimation of the characteristic time for the change of  $t_* \propto b^{-2/3}$ , where  $b$  is the magnetic field gradient [25]. A slow population change, which occurs regardless of  $\Delta\theta$  in the data of Fig. 4, is caused by a residual axial magnetic field gradient  $\partial B_z/\partial z$ . The existence of the axial gradient in these data is confirmed by the fact that the spin components separate in the axial direction at later times. This slow population change can be suppressed by reducing the axial magnetic field gradient. We actually observed population conservation over 400 ms after the gradient adjustment, as will be shown later.

We next observed the change in the atom loss rate. Figure 5 shows the evolution of the atom numbers, corresponding to the data in Figs. 4(b) and 4(d). The decay is faster when

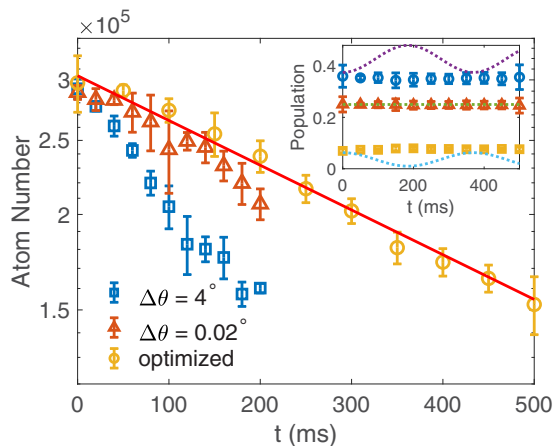


FIG. 5. Atom number losses (semilogarithmic plot). The solid line is an exponential fit to the data with the optimized field gradient. The inset shows the population evolution for the optimized case. The dotted lines are the reference curves of the mean-field-driven evolution within the SMA and assuming no inelastic collisional losses [26].

$\Delta = 4^\circ$  than for  $\Delta \approx 0^\circ$ . In the latter case, the decay rate starts to increase from around  $t = 150$  ms, where the population changes occur [see Fig. 4(f)]. We take different data another day with optimization of  $\theta$  and fine adjustment of the axial *real* magnetic field gradient. The axial gradient is scanned by a step of 0.14 mG/cm to minimize the axial spin separation. No increase in the loss rate is observed at the later time in this case. The  $1/e$  time for the optimized condition is found to be 742(31) ms. The change of the loss rate can be understood from the property of the inelastic collisions in the  $F = 2$  state [27], which is the hyperfine spin changing process to the  $F = 1$  state and leads to spin-dependent atomic loss. Note that the inelastic collisional loss in the stretched state is inhibited due to the restriction of the angular momentum conservation. The break of the stretched state due to the field gradient results in rapid atom losses.

However, the loss still occurs for the optimized condition. Although the remaining loss may be due to the residual field inhomogeneity, it is associated with the spin mixing induced by the quadratic Zeeman energy [26,28]. We compare the experimental result with the model under the single-mode approximation (SMA) [26,28], which is a good starting point to describe typical spin dynamics of a BEC in the stretched state. According to [26], the population evolution in the limit of small quadratic Zeeman energy  $q$  is approximately given by

$$p_0 = \frac{3}{8} \left[ 1 + \frac{q}{2g_1 n} (1 - \cos 4g_1 n t / \hbar) \right], \quad (5)$$

$$p_1 = \frac{1}{4}, \quad (6)$$

$$p_2 = \frac{1}{16} \left[ 1 - \frac{3q}{2g_1 n} (1 - \cos 4g_1 n t / \hbar) \right], \quad (7)$$

where  $g_1 = \frac{4\pi\hbar^2 a_4 - a_2}{m}$ . Populations  $p_0$  and  $p_2$  would undergo oscillations following these equations. We plot curves,

substituting experimental parameters ( $q/h = 1.2$  Hz and  $g_1 n = 1.4$  Hz) into Eqs. (5)–(7) in the inset of Fig. 5. On the other hand, we observe population conservation, shown in the same inset. As the small- $q$  limit and the SMA are not perfectly valid, the curve is only shown as reference. We however note that the population conservation is not expected around  $q \sim g_1 n$  within the SMA under the assumption of no inelastic losses [26,28]. While the discrepancy may partly come from beyond the SMA effect, which can cause very different dynamics, we suppose it is more likely that the population conservation is due to polarization purification by inelastic collisional losses [29]. It should be noted that the observed population conservation contrasts with the case of the  $F = 1$  state, in which the magnitude of the polarization modulates [30].

#### IV. DISCUSSION

The quantum lock-in VLS detection is of practical use in cold-atom experiments. It can be used for evaluating the degree of circular polarization of an optical trap beam at the atomic position, as we have shown. As the vacuum window birefringence introduces a maximum ellipticity of  $10^{-2}$  or  $10^{-1}$  [19], a beam with no special care taken with respect to the *in vacuo* polarization may generate a fictitious field of several nanotesla or a VLS of tens of hertz, even with a shallow trap for ultracold-atom experiments. Quantum lock-in detection is sensitive enough to ensure better linear polarization at the atomic position and therefore will greatly improve the magnetic conditions in cold-atom experiments. The sensitivity is sufficient to suppress the VLS below the requirements for magnetically sensitive experiments, including studies of spinor BECs. Although a homogeneous linear Zeeman shift does not affect the spinor physics due to spin conservation [31], a magnetic field gradient below several  $\mu\text{T}/\text{m}$  is typically required to prevent magnetic polarization and observe the intrinsic magnetic ground state [32] or dynamics. The subhertz VLS resolution of quantum lock-in detection meets this demand.

Reducing the VLS is also important for precise measurements. In addition to a direct energy shift, an inhomogeneous fictitious field is also detrimental to measurement accuracy [33]. A VLS reduction leads to a long coherence time, which is a mandatory requirement for highly sensitive measurements. We have constructed a precise BEC magnetometer using a transversally polarized  $F = 2$  BEC with a long coherence time, realized using VLS elimination as we have shown. Details of the  $F = 2$  BEC magnetometer are presented elsewhere [34].

We finally discuss the sensitivity limitations. The sensitivity of the quantum lock-in detection is essentially the same as that of a Ramsey interferometer with an equal phase accumulation time. As the atom shot noise is dominant over the photon shot noise in typical absorption imaging, the standard quantum limit in the VLS measurement is given by [35,36]

$$\delta\omega = \frac{1}{T\sqrt{N_{\text{tot}}}}. \quad (8)$$

Here we replace the factor  $\frac{2}{\pi}$  in Eq. (3) due to the sinusoidal modulation with the maximal value of 1, which is realized with a rectangular waveform modulation. Substituting  $N_{\text{tot}} = 3 \times 10^5$  and  $T = 30$  ms into Eq. (8), we obtain  $\delta\omega = 2\pi \times 10$  mHz. This is equivalent to a single shot field sensitivity of approximately 1 pT.

For very sensitive detection of the VLS, careful attention should be paid to distinguish the VLS signal and the technical noises, including ac magnetic field fluctuation. The suppression of the ac magnetic effect is realized by using an appropriate modulation frequency at which the noise component is small. In practice, the best parameter is determined to reduce the uncertainty of the background signal without optical power modulation. The narrowing of the detection bandwidth with a large number of pulses should improve the performance, while increasing pulse numbers does not deteriorate the signal. The reduction of the technical noise in the detection, such as the imperfection in the rf pulses and the spin detection, is also mandatory.

#### V. CONCLUSION

We have demonstrated precise detection of a VLS due to an optical trap using the quantum lock-in method. We have applied the detection to eliminating the VLS, to observe the extension of the lifetime of a transversally polarized  $F = 2$  BEC. The attained subhertz resolution is sufficient to suppress the VLS below the required level for magnetically sensitive research, including the study of spinor BECs. Although our demonstration was performed with a BEC, the scope of the detection method is not limited to cold-atom gases; the proposed method can be applied to spin systems such as trapped ions and diamond nitrogen-vacancy centers, where coherent spin control is possible.

#### ACKNOWLEDGMENT

This work was supported by the MEXT Quantum Leap Flagship Program (MEXT Q-LEAP) Grant No. JPMXS0118070326 and JSPS KAKENHI Grant No. JP19K14635.

- 
- [1] R. Grimm, M. Weidemüller, and Y. B. Ovchinnikov, *Adv. At. Mol. Opt. Phys.* **42**, 95 (2000).  
 [2] A. Görlitz, J. M. Vogels, A. E. Leanhardt, C. Raman, T. L. Gustavson, J. R. Abo-Shaer, A. P. Chikkatur, S. Gupta, S. Inouye, T. Rosenband, and W. Ketterle, *Phys. Rev. Lett.* **87**, 130402 (2001).  
 [3] A. L. Gaunt, T. F. Schmidutz, I. Gotlibovych, R. P. Smith, and Z. Hadzibabic, *Phys. Rev. Lett.* **110**, 200406 (2013).  
 [4] I. Bloch, J. Dalibard, and W. Zwerger, *Rev. Mod. Phys.* **80**, 885 (2008).  
 [5] A. Derevianko and H. Katori, *Rev. Mod. Phys.* **83**, 331 (2011).  
 [6] H. Katori, *Nat. Photon.* **5**, 203 (2011).

- [7] D. M. Stamper-Kurn and M. Ueda, *Rev. Mod. Phys.* **85**, 1191 (2013).
- [8] I. H. Deutsch and P. S. Jessen, *Phys. Rev. A* **57**, 1972 (1998).
- [9] J. M. Geremia, J. K. Stockton, and H. Mabuchi, *Phys. Rev. A* **73**, 042112 (2006).
- [10] I. H. Deutsch and P. S. Jessen, *Opt. Commun.* **283**, 681 (2010).
- [11] O. Mandel, M. Greiner, A. Widera, T. Rom, T. W. Hänsch, and I. Bloch, *Phys. Rev. Lett.* **91**, 010407 (2003).
- [12] O. Mandel, M. Greiner, A. Widera, T. Rom, T. W. Hänsch, and I. Bloch, *Nature (London)* **425**, 937 (2003).
- [13] A. Heinz, A. J. Park, N. Šantić, J. Trautmann, S. G. Porsev, M. S. Safronova, I. Bloch, and S. Blatt, *Phys. Rev. Lett.* **124**, 203201 (2020).
- [14] M. V. Romalis and E. N. Fortson, *Phys. Rev. A* **59**, 4547 (1999).
- [15] D. F. Jackson Kimball, J. Dudley, Y. Li, D. Patel, and J. Valdez, *Phys. Rev. D* **96**, 075004 (2017).
- [16] M. Fleischhauer, A. B. Matsko, and M. O. Scully, *Phys. Rev. A* **62**, 013808 (2000).
- [17] G. E. Jellison, *Appl. Opt.* **38**, 4784 (1999).
- [18] K. Zhu, N. Solmeyer, C. Tang, and D. S. Weiss, *Phys. Rev. Lett.* **111**, 243006 (2013).
- [19] A. Steffen, W. Alt, M. Genske, D. Meschede, C. Robens, and A. Alberti, *Rev. Sci. Instrum.* **84**, 126103 (2013).
- [20] D. F. Jackson Kimball, J. Dudley, Y. Li, and D. Patel, *Phys. Rev. A* **96**, 033823 (2017).
- [21] A. A. Wood, L. D. Turner, and R. P. Anderson, *Phys. Rev. A* **94**, 052503 (2016).
- [22] W. H. Yuan, H. L. Liu, W. Z. Wei, Z. Y. Ma, P. Hao, Z. Deng, K. Deng, J. Zhang, and Z. H. Lu, *Rev. Sci. Instrum.* **90**, 113001 (2019).
- [23] S. Kotler, N. Akerman, Y. Glickman, A. Keselman, and R. Ozeri, *Nature (London)* **473**, 61 (2011).
- [24] G. de Lange, D. Ristè, V. V. Dobrovitski, and R. Hanson, *Phys. Rev. Lett.* **106**, 080802 (2011).
- [25] Y. Eto, M. Sadgrove, S. Hasegawa, H. Saito, and T. Hirano, *Phys. Rev. A* **90**, 013626 (2014).
- [26] J. Kronjäger, C. Becker, P. Navez, K. Bongs, and K. Sengstock, *Phys. Rev. Lett.* **100**, 189901(E) (2008).
- [27] S. Tojo, T. Hayashi, T. Tanabe, T. Hirano, Y. Kawaguchi, H. Saito, and M. Ueda, *Phys. Rev. A* **80**, 042704 (2009).
- [28] J. Kronjäger, C. Becker, P. Navez, K. Bongs, and K. Sengstock, *Phys. Rev. Lett.* **97**, 110404 (2006).
- [29] Y. Eto, H. Shibayama, K. Shibata, A. Torii, K. Nabeta, H. Saito, and T. Hirano, *Phys. Rev. Lett.* **122**, 245301 (2019).
- [30] M. Jasperse, M. J. Kewming, S. N. Fischer, P. Pakkiam, R. P. Anderson, and L. D. Turner, *Phys. Rev. A* **96**, 063402 (2017).
- [31] D. M. Stamper-Kurn and W. Ketterle, in *Coherent Atomic Matter Waves*, edited by R. Kaiser, C. Westbrook, and F. David (Springer, Berlin, 2001), pp. 139–217.
- [32] J. Stenger, S. Inouye, D. M. Stamper-Kurn, H.-J. Miesner, A. P. Chikkatur, and W. Ketterle, *Nature (London)* **396**, 345 (1998).
- [33] G. D. Cates, S. R. Schaefer, and W. Happer, *Phys. Rev. A* **37**, 2877 (1988).
- [34] N. Sekiguchi, A. Torii, H. Toda, R. Kuramoto, D. Fukuda, T. Hirano, and K. Shibata, [arXiv:2009.07569](https://arxiv.org/abs/2009.07569).
- [35] V. Giovannetti, S. Lloyd, and L. Maccone, *Science* **306**, 1330 (2004).
- [36] V. Giovannetti, S. Lloyd, and L. Maccone, *Phys. Rev. Lett.* **96**, 010401 (2006).